Engineered Science
DOI: https://dx.doi.org/10.30919/es920

Flexible Carbon Nanotubes/Polystyrene Membranous Composites Toward Ultraweakly and Frequency-Stable Negative Permittivity at kHz Region

Xinxue Tang,[1, 9] Zheng Zhang,[2] D Jaya Prasanna Kuma,[3] Yunpeng Qu,[1,*] Yunchen Long,[4] Peitao Xie,[5, 6,*] Gemeng Liang,[7] Jiaqi Wang,[7] Qingqing Yang,[5] Xiaosi Qi[1,*] and Zhanhu Guo[8]

Abstract

Negative permittivity ($\varepsilon' < 0$) has been a vital and eye-catching electromagnetic parameter for designing new-generation electrical devices. However, ε'-negative materials generally suffer from the overhigh absolute value of ε' and serious frequency dispersion, especially in the radio-frequency region. Hence, carbon nanotubes/polystyrene (CNTs/PS) membranous composites were ingeniously designed and fabricated by a spin-coating procedure. The ultraweakly and frequency-stable negative permittivity ($\varepsilon' \sim -200$) was amazingly achieved over 10 kHz-1 MHz region, attributing to the weakly low-frequency plasmonic state within a 3-dimensional (3D) CNTs network. With increased CNTs content, hopping conduction behavior in composites evolved to metal-like conduction. The impedance analysis based on equivalent circuit models confirmed the inductive characteristic of ε'-negative materials. The obtained flexible CNTs/PS membranous composites could significantly enrich their application on novel wearable electrical devices.

Keywords: Dielectric properties, Membranes, Negative permittivity, Metacomposites.
Received: 12 June 2023; Revised: 29 June 2023; Accepted: 30 June 2023.
Article type: Research article.

1. Introduction

Since the negative permittivity ($\varepsilon' < 0$) concept was first proposed in 1968,[1] various electronic devices for energy storage and transfer system, antenna setup, and electromagnetic wave shielding were found to be related to this physical property.[2-6] As summarized in multiple investigations, the negative value of real permittivity was a common phenomenon in metals, conductive polymers or meticulously constructed metacomposites, ascribed to materials' intrinsic nature related to electron concentration and electron mobility.[6-9] Briefly, high electron concentration is considered to be the vital reason contributing to a strong negative permittivity while electron mobility is closely related to the frequency dispersion. As is known, metals are electron-rich materials that may donate an extremely high negative permittivity value (10^6~10^7) in the metacomposites and meanwhile their absolute value was hard to be manipulated.[10-14] At the same time, a high electron transfer rate due to the enormous carrier concentration has also brought an obvious frequency dispersion in those metacomposites, which may cause more energy loss and block the broadband application in electromagnetic devices.[15,16] Normally, when the absolute value of ε' is less than 1000, it could be a semi-quantifiable criterion and summarized as the "ultraweakly" negative permittivity. Numerous works have concentrated on tunable negative permittivity since strong negative permittivity is generally not an applicable ideal property for electromagnetic devices.

Given the above thinking, many researchers have focused on reducing electron concentration and mobility in metacomposites by introducing another insulator phase into the metals to "dilute" the electron density.[17-21] For example, Choy *et al.* reported metacomposites with 80 wt% copper embedding into epoxy which decreased the absolute value of negative permittivity to ~10^4 order.[22] In 2022, Wang *et al.*

[1] *College of Physics, Guizhou University, Guiyang 550025, China.*
[2] *Department of Applied Mathematics, The Hong Kong Polytechnic University, Hong Kong, China.*
[3] *Department of Chemical Engineering, Ramaiah Institute of Technology, Bengaluru 560054, India.*
[4] *Department of Chemical Engineering, School of Engineering, The University of Manchester, Oxford Road, Manchester M13 9PL, United Kingdom.*
[5] *College of Materials Science and Engineering, Qingdao University, Qingdao 266071, China.*

fabricated nickel/polyaniline metacomposites with ultraweakly negative permittivity (~-10^3), which attributing to the suppress of plasma oscillation in metal network by polyaniline.[23] In fact, the plasma oscillation highly relating to the electron density could be regulated by the meticulously designing of composition and microstructure which could achieve a significantly decreasing of negative value of ε' over the whole test frequency.

Apart from diluting metals' electron concentration, carbon-based materials including well-designed porous carbon, graphene-based nanomaterials, carbon nanotubes (CNTs), and carbon fibers were popularly adopted as conductive filler due to their moderate electron density, as well as their lighter weight for flexible design.[7,24-28] For instance, Wang *et al.* designed the multilayer membranous metacomposites consisting of ε'-negative layers to accomplish frequency-stable dispersion.[29] Among various designs of metacomposites, the insulator phase can be ceramics (Al_2O_3, SiO_2, and $BaTiO_3$).[17,30] and kinds of functional polymers.[31-35] Wherein, polymers have won significant attention for designing percolative composites due to their excellent electrical insulation, lightweight, and greatly mechanical performance.[36,37] By elaborately regulating the component and microstructure, metacomposites can make precise control of dispersion characteristics including response frequency and magnitude of negative permittivity, to satisfy their practical applications in electronic devices.

Once practically applied in a high-frequency electromagnetic field, the serious frequency dispersion of ε'-negative materials would bring an inefficient performance and worse stability in electronic devices. In traditional material selection for radio frequency and lower frequency applications, people focus on metallic materials and their electrical conductivity, rather than the permittivity. Furthermore, the permittivity is often overlooked because it is an imaginary number that is difficult to measure due to the high plasma frequency. To meet the demand for miniaturized electronic component design, metacomposites have become a good choice for low-frequency applications. These materials offer new possibilities for highly integrated electronic devices and can help overcome the limitations of traditional materials for achieving optimal performance in low-frequency electromagnetic fields. Accordingly, the stable ε'-negative response and the relatively smaller absolute value in the shifting frequency range are promising choices for new electronic components to achieve impedance matching, which has been challenging for years.[38-40] In addition, such weakly and stably negative permittivity properties were essential for flexible membranous metacomposites when applied in wearable equipment and flexible electronic devices.[28] (Table 1).

In this work, carbon nanotubes/polystyrene (CNTs/PS) membranous composites were designed and produced by a spin-coating process. A 3-dimensional (3D) CNTs network in membranous composites was gradually constructed. The Drude model and the equivalent circuit analysis were used to illustrate the generation mechanisms of negative permittivity. The hydrophobic CNTs/PS membranous composites with certain toughness and flexibility would be a better choice for wearable electrical devices and electromagnetic wave shielding.

2. Experimental

2.1 Chemicals and characterizations

Polystyrene (PS, Sigma-Aldrich, purity ≥ 99%) and carbon nanotubes (CNTs, length: 5μm, diameter: 25 nm), Dichloromethane (DCM, CH_2Cl_2, Sigma-Aldrich, purity ≥ 99%） were used as received without further purification. The microstructures and morphological evolution of CNTs/PS membranous composites were collected on the FESEM (Hitachi, SU-70, Tokyo, Japan). X-ray diffraction (XRD) data for composites were recorded on a BRUKER SRD-D2 Phaser (2θ = 10-80°, scanning rate of 20°/min). X-ray photoelectron spectroscopy (XPS) was collected on X-ray Photoelectron Spectrometer (PHI Model 5802). By the impedance analyzer (Agilent E4991A), alternating current conductivity (σ_{ac}), dielectric permittivity (ε', ε''), phase angle (θ), and the impedance (Z′, Z") properties of the CNTs/PS membranous composites were recorded respectively. The ε' ($\varepsilon' = Cd/A\varepsilon_0$, $\boldsymbol{C}$, capacitance; d, membranous composite thickness) and ε'' ($\varepsilon'' = d/2\pi fA\varepsilon_0$, f = *frequency*, d = membranous composite thickness; A represents electrode's area; $\boldsymbol{\varepsilon_0}$ = 8.85×10^{-12} F/m) were calculated respectively. $\sigma_{ac} = d/RA$ (R means resistance). The real part (*Re (Z)*, Z') of impedance and the imaginary part (*Im (Z)*, Z'') of impedance were directly read out by the analyzer machine.

2.2 Preparation of CNTs/PS membranous composites

PS was dissolved in DCM to get the pre-stock polymer solution (2 g/6-8 ml). Weighed CNTs of different masses were dispersed into the pre-stock polymer solution respectively, and after an ultrasonic and vortex treatment for 10 min, uniformly dispersed mixtures (CNTs: PS mass weight content: 5 wt%, 10 wt%, 15 wt%, 20 wt%, 30 wt%) were achieved. CNTs/PS

[5] *College of Materials Science and Engineering, Qingdao University, Qingdao 266071, China.*
[6] *Foshan (Southern China) Institute for New Materials, Foshan, 528200, China.*
[7] *School of Chemical Engineering & Advanced Materials, The University of Adelaide, Adelaide, Australia.*
[8] *Integrated Composites Lab, Department of Mechanical and Construction Engineering, Northumbria University, Newcastle Upon Tyne, NE1 8ST, UK.*
[9] *School of Chemical Engineering and Technology, China University of Mining and Technology, Xuzhou 221116, China.*
**Email:* ypqu@gzu.edu.cn (Y. Qu), xiepeitao1991@qdu.edu.cn (P. Xie), xsqi@gzu.edu.cn (X. Qi)

Table 1. Comparison of various ε'-negative materials.

ε'-negative materials	Filling content	Average value of ε'	Stability of ε'	Mechanical performance	ε'- Negative frequency	Refs
Ti_3AlC_2-polyimide	44-88 wt%	~ -10^3	shifting	–	10 MHz-1 GHz	[55]
$La_{0.5}Sr_{0.5}MnO_3$	–	~ -10^5	shifting	–	10 MHz-650 MHz	[52]
$BaTiO_3$/Ag/ epoxy	5wt% (0-1 wt% Ag)	~ -10^7	shifting	–	1 kHz-1 MHz	[17]
Al/acrylic polyurethane	3.58 wt%-86.41wt%	~ -10^2	shifting	Flexible	10 MHz-800 MHz	[12]
Ag/SiO_2	17-37 wt%	~ -10^3	shifting	–	10 MHz-520 MHz	[56]
Cu/epoxy	10-80 wt%	~ -10^4	shifting	–	10 kHz-1 MHz	[22]
Graphene/$CaCu_3Ti_4O_{12}$	1-16 wt%	~ -10^3	shifting	–	10 MHz-1 GHz	[54]
MWCNTs/Al_2O_3	1-12 wt%	~ -10^2	shifting	–	10 MHz-350 MHz	[19]
Graphene/polypyrrole	10-70 wt%	~ -10^2	shifting	–	1 MHz-1 GHz	[32]
MWCNTs /PVA	3 -15 wt%	~ -10^2	shifting	Flexible	580 kHz-1 MHz	[37]
Graphene /PVDF	2-18 wt%	~ -10^3	stable	–	100 kHz-1 MHz	[29]
MWCNTs/PANI	10-90 wt%	~ -10^2	shifting	–	100 MHz-1 GHz	[24]
CNTs/PS	5-30 wt%	~ -10^2	stable	Flexible	10 kHz-1 MHz	This work

membranous composites were produced by a spin coating procedure (spin-coater CY-SP-3) and the thick and sticky CNTs dispersion was spread evenly with the spin rate at 400 rpm/min. After being coated on the glass substrate, the DCM in the wet membranous composites was evaporated at room temperature (20 °C) for 10 hours and the black and plain membranous composites were able to be peeled off from the substrate (Fig. 1a). The light, durable and flexible membranous composite could be cropped and remolded into desired shapes by multi-folding, bending, and cutting without

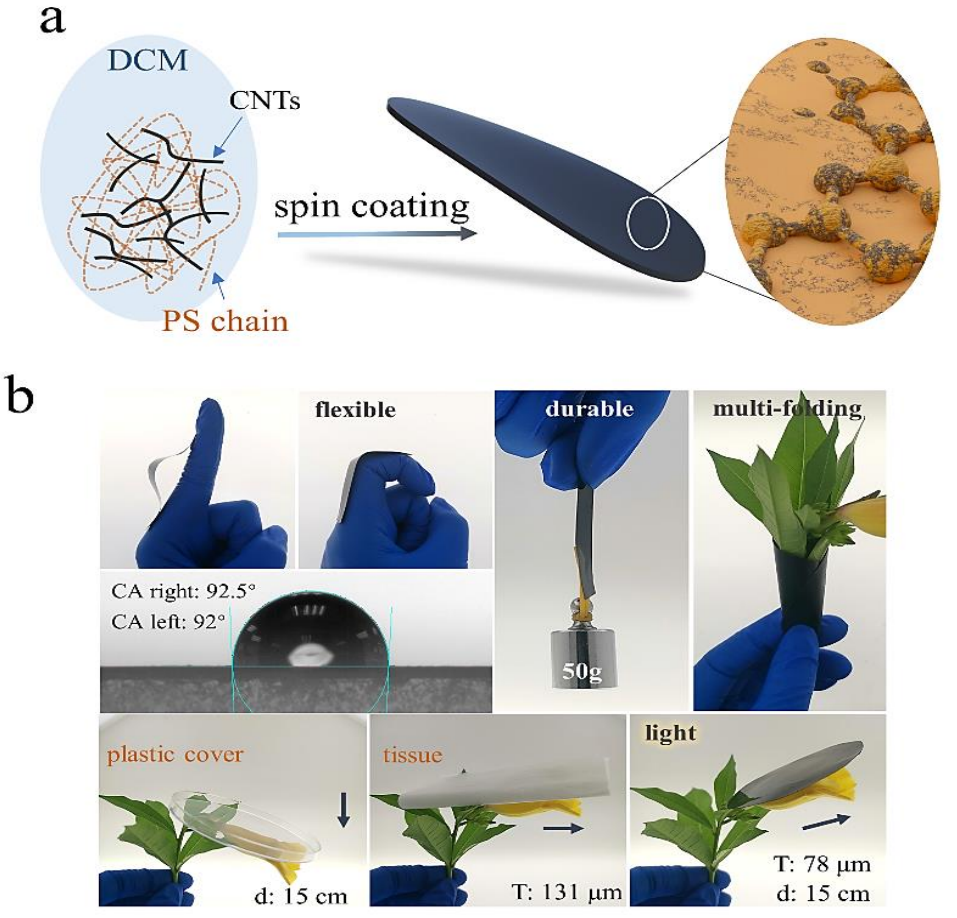

Fig. 1 The experimental process sketch for CNTs/PS membranous composites (a). The flexibility and wettability of CNTs/PS membranous composites: the light membranous composite could be multi-folding, bending, and cutting freely. The contact angle was about 92°. (d: diameter, T: thickness, plastic cover: commercial petri dish cover, tissue: double layer lens cleaning tissue) (b).

ruining the inner network and conductive micro-structures (Fig. 1b).

3. Results and discussion

3.1 Microstructure of CNTs/PS membranous composites

Microstructures of CNTs/PS membranous composites with different CNTs content were collected and presented in Fig. 2a. PS matrix formed a completely tight layer structure when no CNTs joined the polymer. When increasing the CNTs content from 5 wt% to 15 wt%, fiber-shape CNTs (purple area) in the PS layers (brown-yellow arrow) have gradually been presented and the area-distributed CNTs implied an expanding conductive area in the insulative matrix started to be built. The connected CNTs network could be noticed in the 20 wt% membranous composites in the SEM images since the fiber crossed through the polymer matrix directedly. After 30 wt% content of CNTs were introduced into the polymer matrix, a stacked and connected 3D CNTs network was notably covering the matrix surface and filling the interspace (Fig. 2a). Such distribution has reversed the PS-covered membranous appearance in 5 wt%-CNTs composites and obviously depicted the CNTs networks establishment in the membranous films. XRD patterns for CNTs/PS membranous composites were shown in Fig. 2b and the typical diffraction peaks for CNTs (002) and (100) were gradually strengthened along with the increase of the CNTs content, implying the expanded CNTs and PS interface (Fig. 2b). The C1s XPS spectrum for CNTs was depicted in Fig. 2c and the peak at binding energy (BE) of 284.9 eV and 285.8 eV were attributed to the C-C (sp^2) and C-C(sp^3) by the carbon-carbon interaction.[41] The peak at BE of 291.4 eV was due to the π-π* plasmon in the benzene rings of membranous composites from CNTs.[42,43] Besides the great flexibility, the wettability of the membranous composites' surface has been recorded by the contact angle tester as 92°, which presented the good hydrophobic character. All the mentioned properties of CNTs/PS membranous composites may broaden their applications in water-shielding electrical materials.[44-46] (Fig. 1b).

3.2 Dielectric properties of the CNTs/PS membranous composites

The real permittivity (ε') and imaginary permittivity (ε'') spectra for membranous composites with different CNTs content were shown in Fig. 3. For composites with 5 wt% to 20 wt% content of CNTs, the ε' value was positive and experienced a gentle improvement that could be explained by the Maxwell–Wagner Sillars effect.[47-49] Specifically, the CNTs was surrounded and isolated by PS layers which could be equivalent to hundreds of micro-capacitors. Furthermore, there was an interfacial polarization effect in composites, that is, many charge carriers were accumulated at the interface of CNTs and PS under an external electric field. As the content

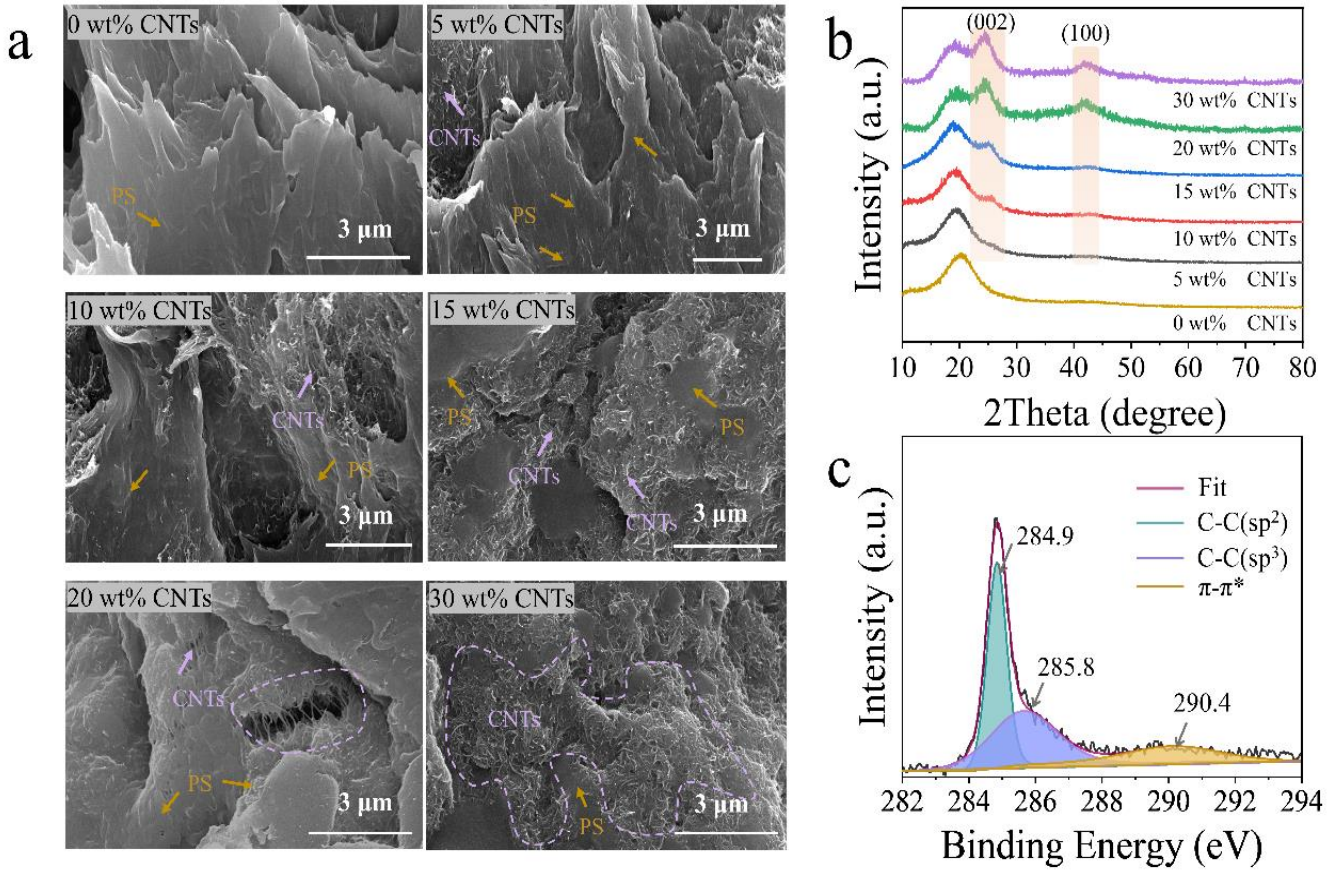

Fig. 2 SEM images for 0-30 wt% CNTs content CNTs/PS membranous composites (a). XRD patterns of CNTs/PS membranous composites(b); XPS spectrum of CNTs (c).

of CNTs increased from 5 wt% to 20 wt%, the equivalent micro-capacitor area and interfacial polarization effect have been expanded, leading to the enhanced positive permittivity performance. As shown in Fig. 3a, the ε' values decreased with increasing test frequency ascribing to the dielectric relaxation behavior.[50]

After the CNTs content increased to 30 wt%, the ε' value became negative, implying a 3D conductive CNTs network in the CNTs/PS membranous composite. The relationship between ε' and frequency was well-fitted and explained by the Drude model:[20]

$$\varepsilon'_r(\omega) = 1 - \frac{\omega_p^2}{\omega^2 + \Gamma_D^2} \quad (1)$$

$$\omega_p = \sqrt{\frac{n_{eff}e^2}{m_{eff}\varepsilon_0}} \quad (2)$$

$\omega_p(\omega_p = 2\pi f_p)$: angular plasma frequency, (f_p, the plasma frequency),
$\omega(\omega = 2\pi f)$: angular frequency of the applied electrical field,
Γ_D: damping constant,
ε_0: 8.85×10^{-12} F/m,
n_{eff}: effective concentration of free electrons,
m_{eff}: effective weight of electron,
e: electron charge (1.6×10^{-19} C).

As depicted in the formula (2), the effective electron concentration and electron weight are two important parameters that will change the ω_p and further influence negative permittivity, as well as the frequency dispersion. With the conductive CNTs content increase, the effective concentration and weight of free electrons would strengthen the plasma oscillation effect in CNTs/PS metacomposite and further lead to the upgraded ω_p.[51-54] The absolute value of ε' (30 wt% CNTs/PS membranous composite) was as low as about 200 with a frequency-stable dispersion from 1 kHz to 1MHz, showing competitive ε'-negative property, frequency stability, and mechanical performance compared to the reported metacomposites in Table 1.

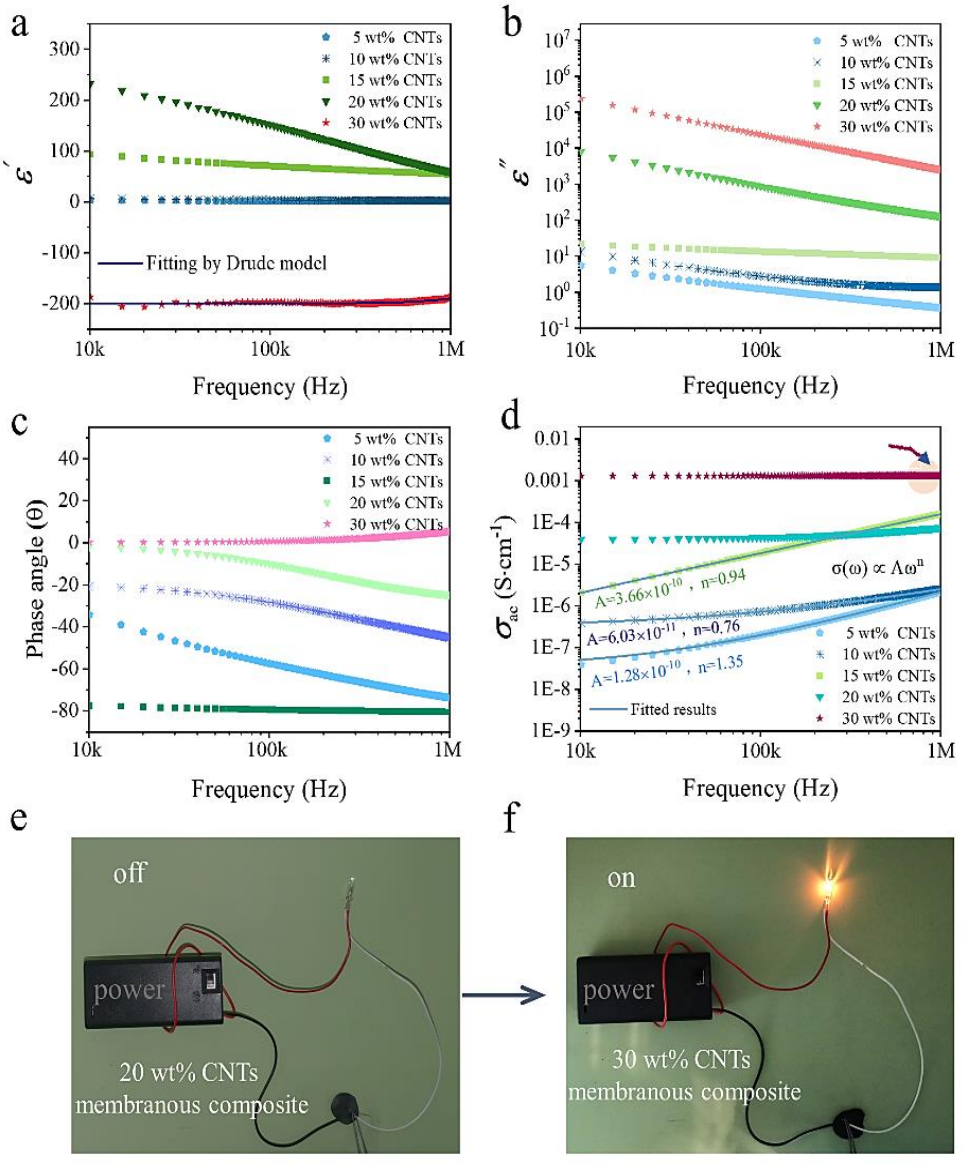

Fig. 3 Frequency dependences of (a) ε', (b) ε'', (c) θ and (d) σ_{ac} for the CNTs/PS membranous composites, the electrical percolation effect of membranous composites (e-f).

Normally, imaginary permittivity (ε'') was adopted to explain the dielectric loss in the composite materials, which was the collaboration result of the interfacial polarization effect and electrical conduction process in different materials.[57,58] As presented in Fig. 3b, the ε'' value increased with increasing CNTs content, suggesting an enhancement of dielectric loss in membranous composites. In composites with 5-15 wt% CNTs content, the interfacial polarization effect was the primary source for dielectric loss. When the CNTs content increased to 30wt%, the conduction loss played the main role in dielectric loss which exactly corresponding to the formed 3D conductive CNTs network in composites.

Both positive permittivity and negative phase angle (θ) could confirm the capacitive behavior in the equivalent circuit. In contrast, the negative permittivity and positive phase angle indicated the inductive characters. In composites of 5-20 wt% CNTs content, the θ value was negative within the test frequency, indicating that voltage lags current, which was consistent with the positive permittivity shown in Fig. 3a. When the CNTs content increased to 30 wt%, the phase angle changed to positive value along with negative permittivity behavior. As presented in Fig. 3c, the negative permittivity of membranous composites showed the positive θ value, indicating a reverse dielectric response compared to ε'-positive materials.[56]

For CNTs/PS composites, alternating current conductivity (σ_{ac}) changed with CNTs content, as well as increasing frequency (Fig. 3d). The σ_{ac} of composites increased with the enhanced CNTs clusters from 5 wt% to 30 wt% content of CNTs. For composites at low CNTs content, the connectivity and conductivity were interrupted by the insulating polymer which resulted in a low σ_{ac} value around 10^{-7}-10^{-5} ($S{\cdot}cm^{-1}$) and an unconnected circuit (Fig. 3e). Further increasing the CNTs content, the conductive CNTs network was constructed and continuously promoted the σ_{ac} value to 10^{-2} ($S{\cdot}cm^{-1}$) along with conductive circuit with a light bulb (Fig. 3f). Apart from the influence of CNTs content, the σ_{ac} climbed up with gradually changing frequency from 10 kHz to 1MHz that well-fitted by the Jonscher power law[29]: $\sigma(\omega) \propto A\omega^n$ (where $\omega = 2\pi f$ is the angular frequency, n is the fractional exponent, and A is the pre-exponential factor) and the fitting results were presented in the figure. These shifting trends indicated a hopping conduction behavior in membranous composites (5-20 wt% CNTs) that the electrons "jumped" from the host to neighbored CNTs under the electric field (Fig. 4). When CNTs content reached 20 wt%, a direct current (dc) conductivity plateau and higher σ_{ac} were presented, showing a dc conductivity behavior and occurrence of percolation. In composite of 30 wt% CNTs, the σ_{ac} slightly decreased in the high-frequency region (insert in Fig. 3d), implying a metal-like conduction along with skin effect that the electrons quickly transferred in low depth.[51,55] Different σ_{ac} changing rules were consistent with the percolative microstructure of CNTs/PS composites as shown in Fig. 2a. Continuously increasing CNTs successfully bridged the insulated PS matrix and finally contributed to a stacked and continuous 3-dimensional network after 30 wt% content CNTs reached.

The percolative evolution process of CNTs/PS metacomposites under an alternative external electrical field was exhibited in Fig. 4. The charge carriers between CNTs and PS were accumulated through interfacial polarization under an electrical field and the hopping conduction were achieved for composites at low CNTs content. With increasing CNTs content, the isolated CNTs tend to be clusters and the interfacial polarization was gradually enhanced, leading to obviously improvement of positive ε', as shown in Fig. 3a. Typically, the decreasing trend of positive ε' with increasing frequency originated from the leakage current within the CNTs clusters. When the CNTs content increased to 30 wt%, the 3D CNTs network was formed and the low-frequency plasma oscillation was strengthened, triggering the transition from hopping conduction to metal-like conduction, while causing the ε'-negative response over whole test frequency band.

3.3 Impedance and equivalent circuit simulation for CNTs/PS membranous composites

Dielectric materials exposed to the alternating electric field might work as capacitors (C), inductors (L), or resistors (R) as well as the combined groups. Real and imaginary impedance (Z) spectra of CNTs/PS membranous composites were analyzed by equivalent circuits to clarify the electrical character of ε'-negative materials. Chi-square values are commonly accepted to compare the correlation between experimental data and simulated values, the smaller the Chi-square value is, the more accurate the equivalent circuit fit. As shown in Figs. 5a-c, the imaginary impedance Im (Z) kept a negative value over the test frequency (10 kHz to 1MHz) for composites with 5 wt%, 10 wt%, and 20 wt% CNTs content. The fitted lines were also shown in the figures according to the simulation data. The Chi-square values were 1.23×10^{-5}, $1.23 \times 10^{-5,}$ and 8.24×10^{-7}, respectively. The capacitors (C) in the equivalent circuit attribute to the equivalent micro-capacitors consisting of CNTs and PS matrix, that is, isolated CNTs separated by the insulating PS, as discussed in the microstructural evolution of CNTs/PS composites. Thus, ε'-positive CNTs/PS composites could be considered as capacitive dielectrics, which shows promising applications in miniaturized and flexible energy storage devices.

Interestingly, as displayed in Fig. 5d, composite with 30 wt% CNTs content shows positive value of Im (Z) over 10 kHz-1 MHz regions. In contrast, the inductors appeared in the simulated equivalent circuit which specifically assembled by the capacitor (C), three resistors (R_1, R_2 and R_3) and two inductors (L_1 and L_2). The Chi-square for the fitting curve was as low as 1.06×10^{-5}, indicating a good consistency with the dielectric performance. The employment of inductors indicates that ε'-negative CNTs/PS composites are intrinsically inductive which could be applied on new-generation wearable coil-less electrical inductors, *etc*.

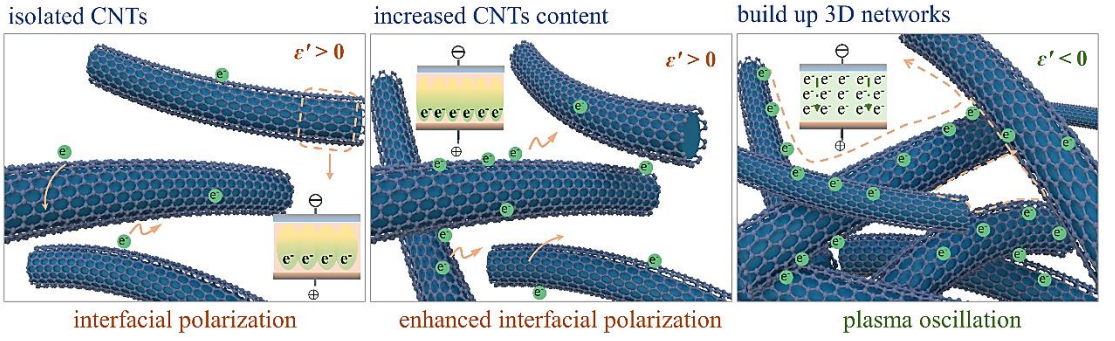

Fig. 4 Evolution process schematic and generation mechanism of negative permittivity.

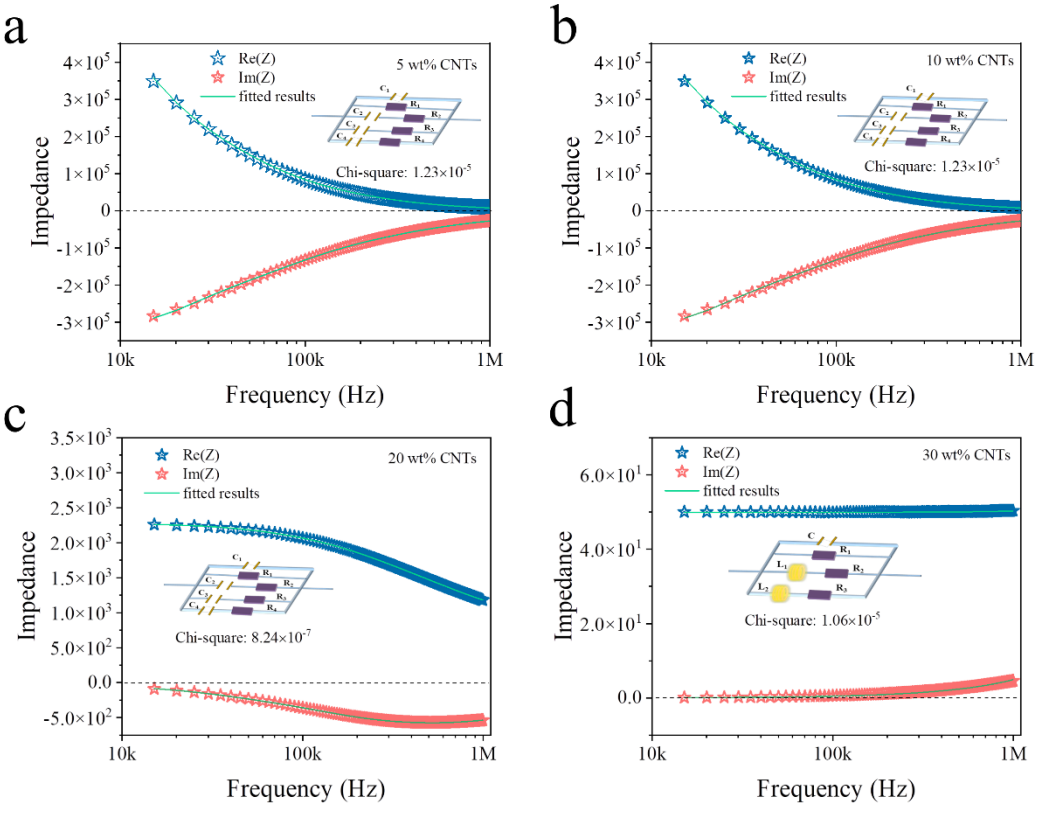

Fig. 5 Impedance spectra and equivalent circuits model of the CNTs/PS membranous composites (a-d).

4. Conclusion

In summary, flexible CNTs/PS membranous composites achieved ultraweakly and frequency-stable negative permittivity (ε' ~ -200) over the 10 kHz-1 MHz band. Increasing CNTs content from 5 wt% to 30 wt% in membranous composites has gradually bridged the CNTs network in the insulated PS polymer. Established 3D CNTs network in composites realized the metal-like conduction. The impedance analysis based on equivalent circuit models with low Chi-square value successfully confirmed the inductive characteristic of ε'-negative metacomposites. The flexible hydrophobic CNTs/PS membranous composites with ultraweakly and frequency-stable negative ε' properties will enrich choices for wearable electrical applications.

Acknowledgments

This work was financially supported by the Natural Science Foundation of Shandong Province [No. ZR2020QE006], National Natural Science Foundation of China [No. 52101176], the Fund of Natural Science Special (Special Post) Research Foundation of Guizhou University [Grant No. 2023-032].

Conflict of Interest

There is no conflict of interest.

Supporting Information

Not applicable.

References

[1] V. G. Veselago, The electrodynamics of substances with simultaneously negative values of ε and μ, *Soviet Physics Uspekhi*, 1968, **10**, 509-514, doi:

10.1070/pu1968v010n04abeh003699.
[2] L. Sun, Z. Shi, B. He, H. Wang, S. Liu, M. Huang, J. Shi, D. Dastan, H. Wang, Asymmetric trilayer all-polymer dielectric composites with simultaneous high efficiency and high energy density: a novel design targeting advanced energy storage capacitors, *Advanced Functional Materials*, 2021, **31**, 2100280, doi: 10.1002/adfm.202100280.
[3] A. Xie, J. Fu, R. Zuo, X. Jiang, T. Li, Z. Fu, Y. Yin, X. Li, S. Zhang, Supercritical relaxor nanograined ferroelectrics for ultrahigh-energy-storage capacitors, *Advanced Materials*, 2022, **34**, 2204356, doi: 10.1002/adma.202204356.
[4] Z. Wei, G. Zhang, X. Song, Y. Wang, H.Wang, M. Gao, H.Tian, W. Cai, Yao Liu, Z. Wang, Z. Zhang. R. Fan, Metallic State and Negative Permittivity in $LaCo_{1-x}Ni_xO_3$ Ceramics, *Engineered Science*, 2023, **21**, 806, doi: 10.30919/es8d806.
[5] Z. Hanani, D. Mezzane, M. Amjoud, M. Lahcini, M. Spreitzer, D. Vengust, A. Jamali, M. El Marssi, Z. Kutnjak, M. Gouné, The paradigm of the filler's dielectric permittivity and aspect ratio in high-k polymer nanocomposites for energy storage applications, *Journal of Materials Chemistry C*, 2022, **10**, 10823-10831, doi: 10.1039/d2tc00251e.
[6] Jun-Wei, Zha, Polymer-based dielectrics with high permittivity for electric energy storage: a review, *Nano Energy*, 2021, **89**, 106438, doi: 10.1016/j.nanoen.2021.106438.
[7] X. Zhang, X. Yan, Q. He, H. Wei, J. Long, J. Guo, H. Gu, J. Yu, J. Liu, D. Ding, L. Sun, S. Wei, Z. Guo, Electrically conductive polypropylene nanocomposites with negative permittivity at low carbon nanotube loading levels, *ACS Applied Materials & Interfaces*, 2015, **7**, 6125-6138, doi: 10.1021/am5082183.
[8] J. Wang, Z. Shi, F. Mao, S. Chen, X. Wang, Bilayer polymer metacomposites containing negative permittivity layer for new high-k materials, *ACS Applied Materials & Interfaces*, 2017, **9**, 1793-1800, doi: 10.1021/acsami.6b12786.
[9] H. Wu, Y. Qi, Z. Wang, W. Zhao, X. Li, L. Qian, Low percolation threshold in flexible graphene/acrylic polyurethane composites with tunable negative permittivity, *Composites Science and Technology*, 2017, **151**, 79-84, doi: 10.1016/j.compscitech.2017.08.011.
[10] M.-Z. Fan, B.-Z. Sun, J.-Y. Jiang, J.-Y. Pan, P.-H. Hu, Enhanced energy density in polyetherimide nanocomposite film at high temperature induced by electrospun $BaZrTiO_3$ nanofibers, *Rare Metals*, 2023, **42**, 1912-1922, doi: 10.1007/s12598-022-02241-5.
[11] F. R. G. Bagsican, M. Wais, N. Komatsu, W. Gao, L. W. Weber, K. Serita, H. Murakami, K. Held, F. A. Hegmann, M. Tonouchi, J. Kono, I. Kawayama, M. Battiato, Terahertz excitonics in carbon nanotubes: exciton autoionization and multiplication, *Nano Letters*, 2020, **20**, 3098-3105, doi: 10.1021/acs.nanolett.9b05082.
[12] Z. Wang, K. Sun, P. Xie, Y. Liu, Q. Gu, R. Fan, Permittivity transition from positive to negative in acrylic polyurethane-aluminum composites, *Composites Science and Technology*, 2020, **188**, 107969, doi: 10.1016/j.compscitech.2019.107969.
[13] Wook, Kim, Interfacial molecular engineering for enhanced polarization of negative tribo-materials, *Nano Energy*, 2022, **96**, 107110, doi: 10.1016/j.nanoen.2022.107110.
[14] Y. Chu, S. Nie, S. Liu, C. Lee, B. Bate, Complex dielectric permittivity of metal and polymer modified montmorillonite, *Journal of Hazardous Materials*, 2019, **374**, 382-391, doi: 10.1016/j.jhazmat.2019.04.066.
[15] Z. Wei, Z. Wang, C. Xu, G. Fan, X. Song, Y. Liu, R. Fan, Defect-induced insulator-metal transition and negative permittivity in La1-Ba CoO3 perovskite structure, *Journal of Materials Science & Technology*, 2022, **112**, 77-84, doi: 10.1016/j.jmst.2021.11.002.
[16] M. Man, V. K. Sharma, E. A. Kumar, V. Gayathri, Hydrogen storage in carbon materials—a review, *Energy Storage*, 2019, **1**, e35, doi: 10.1002/est2.35.
[17] M. Han, Z. Shi, W. Zhang, K. Zhang, H. Wang, D. Dastan, R. Fan, Significantly enhanced high permittivity and negative permittivity in $Ag/Al_2O_3/3D\text{-}BaTiO_3$/epoxy metacomposites with unique hierarchical heterogeneous microstructures, *Composites Part A: Applied Science and Manufacturing*, 2021, **149**, 106559, doi: 10.1016/j.compositesa.2021.106559.
[18] C. Cheng, Y. Jiang, X. Sun, J. Shen, T. Wang, G. Fan, R. Fan, Tunable negative permittivity behavior and electromagnetic shielding performance of silver/silicon nitride metacomposites, *Composites Part A: Applied Science and Manufacturing*, 2020, **130**, 105753, doi: 10.1016/j.compositesa.2019.105753.
[19] C. Cheng, R. Fan, Y. Ren, T. Ding, L. Qian, J. Guo, X. Li, L. An, Y. Lei, Y. Yin, Z. Guo, Radio frequency negative permittivity in random carbon nanotubes/alumina nanocomposites, Nanoscale, 2017, **9**, 5779-5787, doi: 10.1039/c7nr01516j.
[20] H. Wu, R. Yin, L. Qian, Z. Zhang, Three-dimensional graphene network/phenolic resin composites towards tunable and weakly negative permittivity, *Materials & Design*, 2017, **117**, 18-23, doi: 10.1016/j.matdes.2016.12.068.
[21] H. Wu, Y. Zhang, R. Yin, W. Zhao, X. Li, L. Qian, Magnetic negative permittivity with dielectric resonance in random Fe3O4@graphene-phenolic resin composites, *Advanced Composites and Hybrid Materials*, 2018, **1**, 168-176, doi: 10.1007/s42114-017-0014-1.
[22] K. Sun, J. Xin, Y. Li, Z. Wang, Q. Hou, X. Li, X. Wu, R. Fan, K. Leong Choy, Negative permittivity derived from inductive characteristic in the percolating Cu/EP metacomposites, *Journal of Materials Science & Technology*, 2019, **35**, 2463-2469, doi: 10.1016/j.jmst.2019.07.015.
[23] Yunpeng, Qu, Ultraweakly and fine-tunable negative permittivity of polyaniline/nickel metacomposites with high-frequency diamagnetic response, *Composites Science and Technology*, 2022, **217**, 109092, doi: 10.1016/j.compscitech.2021.109092.
[24] Xiuchao, Yao, Multi-walled carbon nanotubes/polyaniline composites with negative permittivity and negative permeability, *Carbon*, 2016, **107**, 261-267, doi: 10.1016/j.carbon.2016.05.055.
[25] H. Wu, X. Huang, L. Qian, Recent progress on the metacomposites with carbonaceous fillers, *Engineered Science*, 2020, **2**, 17-25, doi: 10.30919/es8d656.
[26] R. Singh, A. Chakravarty, S. Mishra, R. C. Prajapati, J. Dutta,

I. K. Bhat, U. Pandel, S. K. Biswas, K. Muraleedharan, AlN-SWCNT metacomposites having tunable negative permittivity in radio and microwave frequencies, *ACS Applied Materials & Interfaces*, 2019, **11**, 48212-48220, doi: 10.1021/acsami.9b15909.
[27] X. Hong, X. Wang, Y. Li, J. Fu, B. Liang, Sandwich structured MnO_2/carbon nanosheet/MnO_2 composite for high-performance supercapacitors, *Journal of Alloys and Compounds*, 2021, **889**, 161821, doi: 10.1016/j.jallcom.2021.161821.
[28] H. Wu, H. Sun, F. Han, P. Xie, Y. Zhong, B. Quan, Y. Zhao, C. Liu, R. Fan, Z. Guo, Negative permittivity behavior in flexible carbon nanofibers- polydimethylsiloxane films, *Engineered Science*, 2021, **17**, 113-120, doi: 10.30919/es8d576.
[29] Zongxiang, Wang, Negative-k and positive-k layers introduced into graphene/polyvinylidene fluoride composites to achieve high-k and low loss, *Materials & Design*, 2021, **209**, 110009, doi: 10.1016/j.matdes.2021.110009.
[30] S.-X. Zhang, J.-C. Wang, Y.-M. Zhao, Y.-L. Han, A.-J. Ming, F. Wei, C.-H. Mao, High-dielectric loss black silicon decorated with multi-nanostructure for wide-band mid-infrared absorption, *Rare Metals*, 2023, **42**, 2447-2456, doi: 10.1007/s12598-023-02292-2.
[31] L. Sun, N. Wu, R. Peng, Negative dielectric permittivity of PVDF nanocomposites induced by carbon nanofibers and polymer crystallization, *Journal of Applied Polymer Science*, 2020, **137**, 49582, doi: 10.1002/app.49582.
[32] G. Qin, J. Qiu, Graphene/polypyrrole nanocomposites with high negative permittivity and low dielectric loss tangent, *Ceramics International*, 2019, **45**, 5407-5412, doi: 10.1016/j.ceramint.2018.11.241.
[33] H. Luo, J. Qiu, Carbon nanotube/polyolefin elastomer metacomposites with adjustable radio-frequency negative permittivity and negative permeability, *Advanced Electronic Materials*, 2019, **5**, 1900011, doi: 10.1002/aelm.201900011.
[34] H. Gu, H. Zhang, C. Ma, S. Lyu, F. Yao, C. Liang, X. Yang, J. Guo, Z. Guo, J. Gu, Polyaniline assisted uniform dispersion for magnetic ultrafine Barium ferrite nanorods reinforced epoxy metacomposites with tailorable negative permittivity, The *Journal of Physical Chemistry C*, 2017, **121**, 13265-13273, doi: 10.1021/acs.jpcc.7b03580.
[35] F. Yao, W. Xie, M. Yang, H. Zhang, H. Gu, A. Du, N. Naik, D. P. Young, J. Lin, Z. Guo, Interfacial polymerized copolymers of aniline and phenylenediamine with tunable magnetoresistance and negative permittivity, *Materials Today Physics*, 2021, **21**, 100502, doi: 10.1016/j.mtphys.2021.100502.
[36] H. Luo, X. Zhou, C. Ellingford, Y. Zhang, S. Chen, K. Zhou, D. Zhang, C. R. Bowen, C. Wan, Interface design for high energy density polymer nanocomposites, *Chemical Society Reviews*, 2019, **48**, 4424-4465, doi: 10.1039/c9cs00043g.
[37] J. Tian, R. Fan, Z. Zhang, Y. Li, H. Wu, P. Yang, P. Xie, W. Duan, C.-S. Lee, Flexible and biocompatible poly (vinyl alcohol)/multi-walled carbon nanotubes hydrogels with epsilon-near-zero properties, *Journal of Materials Science & Technology*, 2022, **131**, 91-99, doi: 10.1016/j.jmst.2022.05.019.
[38] P. Xie, Z. Wang, Z. Zhang, R. Fan, C. Cheng, H. Liu, Y. Liu, T. Li, C. Yan, N. Wang, Z. Guo, Silica microsphere templated self-assembly of a three-dimensional carbon network with stable radio-frequency negative permittivity and low dielectric loss, *Journal of Materials Chemistry C*, 2018, **6**, 5239-5249, doi: 10.1039/c7tc05911f.
[39] K. Sun, W. Duan, Y. Lei, Z. Wang, J. Tian, P. Yang, Q. He, M. Chen, H. Wu, Z. Zhang, R. Fan, Flexible multi-walled carbon nanotubes/polyvinylidene fluoride membranous composites with weakly negative permittivity and low frequency dispersion, *Composites Part A: Applied Science and Manufacturing*, 2022, **156**, 106854, doi: 10.1016/j.compositesa.2022.106854.
[40] W. Han, F. Gao, L. Zhou, L. Wang, X. Hua, X. Xue, Z. Li, W. Luo, L. Pang, R. Wei, Flexible fluorinated multi-walled carbon nanotube/polyarylene ether nitrile metacomposites with negative permittivity, *Journal of Materials Chemistry C*, 2022, **10**, 171-179, doi: 10.1039/d1tc03831a.
[41] G. Greczynski, L. Hultman, Referencing to adventitious carbon in X-ray photoelectron spectroscopy: can differential charging explain C1 s peak shifts? , *Applied Surface Science*, 2022, **606**, 154855, doi: 10.1016/j.apsusc.2022.154855.
[42] R. Blume, D. Rosenthal, J.-P. Tessonnier, H. Li, A. Knop-Gericke, R. Schlögl, Characterizing graphitic carbon with X-ray photoelectron spectroscopy: a step-by-step approach, *ChemCatChem*, 2015, **7**, 2871-2881, doi: 10.1002/cctc.201500344.
[43] G. Moraitis, Z. Špitalský, F. Ravani, A. Siokou, C. Galiotis, Electrochemical oxidation of multi-wall carbon nanotubes, *Carbon*, 2011, **49**, 2702-2708, doi: 10.1016/j.carbon.2011.02.060.
[44] J. Ma, Q. Zhao, Y. Zhou, P. He, H. Pu, B. Song, S. Pan, Y. Wang, C. Wang, Hydrophobic wrapped carbon nanotubes coated cotton fabric for electrical heating and electromagnetic interference shielding, *Polymer Testing*, 2021, **100**, 107240, doi: 10.1016/j.polymertesting.2021.107240.
[45] H. Zhang, D.-Z. Zhang, D.-Y. Wang, Z.-Y. Xu, Y. Yang, B. Zhang, Flexible single-electrode triboelectric nanogenerator with MWCNT/PDMS composite film for environmental energy harvesting and human motion monitoring, *Rare Metals*, 2022, **41**, 3117-3128, doi: 10.1007/s12598-022-02031-z.
[46] G. Reddy, R. Katakam, K. Devulapally, L. A. Jones, E. Della Gaspera, H. M. Upadhyaya, N. Islavath, L. Giribabu, Ambient stable, hydrophobic, electrically conductive porphyrin hole-extracting materials for printable perovskite solar cells, *Journal of Materials Chemistry C*, 2019, **7**, 4702-4708, doi: 10.1039/c9tc00605b.
[47] J. Cao, D. Zhang, C. Gu, X. Zhang, M. Okhawilai, S. Wang, J. Han, J. Qin, Y. Huang, Modulating Zn deposition via ceramic-cellulose separator with interfacial polarization effect for durable zinc anode, *Nano Energy*, 2021, **89**, 106322, doi: 10.1016/j.nanoen.2021.106322.
[48] J. Gao, Z.-J. Ma, F.-L. Liu, X.-Y. Weng, Synthesis and electromagnetic wave absorption properties of Gd-Co ferrite@carbon core-shell structure composites, *Rare Metals*, 2023, **42**, 254-262, doi: 10.1007/s12598-022-02123-w.
[49] C. Cheng, R. Fan, Y. Ren, T. Ding, L. Qian, J. Guo, X. Li, L. An, Y. Lei, Y. Yin, Z. Guo, Radio frequency negative permittivity in random carbon nanotubes/alumina nanocomposites,

Nanoscale, 2017, **9**, 5779-5787, doi: 10.1039/c7nr01516j.
[50] F.-M. Xie, J.-X. Zhou, Y.-Q. Li, J.-X. Tang, Effects of the relative position and number of donors and acceptors on the properties of TADF materials, *Journal of Materials Chemistry C*, 2020, **8**, 9476-9494, doi: 10.1039/d0tc02252g.
[51] M. Liu, H. Wu, Y. Wu, P. Xie, R. A. Pashameah, H. M. Abo-Dief, S. M. El-Bahy, Y. Wei, G. Li, W. Li, G. Liang, C. Liu, K. Sun, R. Fan, The weakly negative permittivity with low-frequency-dispersion behavior in percolative carbon nanotubes/epoxy nanocomposites at radio-frequency range, *Advanced Composites and Hybrid Materials*, 2022, **5**, 2021-2030, doi: 10.1007/s42114-022-00541-z.
[52] K. Yan, L. Shen, F. Yin, G. Qi, X. Zhang, R. Fan, N. Bao, Metallic ferromagnet of La0.5Sr0.5MnO3 with negative permittivity and permeability, *Advanced Electronic Materials*, 2022, **8**, 2101020, doi: 10.1002/aelm.202101020.
[53] Z. Wang, K. Sun, P. Xie, R. Fan, Y. Liu, Q. Gu, J. Wang, Low-loss and temperature-stable negative permittivity in $La_{0.5}Sr_{0.5}MnO_3$ ceramics, *Journal of the European Ceramic Society*, 2020, **40**, 1917-1921, doi: 10.1016/j.jeurceramsoc.2020.01.024.
[54] Y. Qu, Y. Du, G. Fan, J. Xin, Y. Liu, P. Xie, S. You, Z. Zhang, K. Sun, R. Fan, Low-temperature sintering graphene/$CaCu_3Ti_4O_{12}$ nanocomposites with tunable negative permittivity, *Journal of Alloys and Compounds*, 2019, **771**, 699-710, doi: 10.1016/j.jallcom.2018.09.049.
[55] H. Wu, Z. Mu, G. Qi, Y. Zhang, X. Wang, P. Xie, N. Wu, H. Yuan, K. Sui, R. Fan, C. Liu, Negative permittivity behavior in Ti_3AlC_2-polyimide composites and the regulation mechanism, *Journal of Materials Science: Materials in Electronics*, 2021, **32**, 10388-10397, doi: 10.1007/s10854-021-05695-y.
[56] P. Xie, Z. Zhang, Z. Wang, K. Sun, R. Fan, Targeted double negative properties in silver/silica random metamaterials by precise control of microstructures, *Research*, 2019, **2019**, 1-11, doi: 10.1155/2019/1021368.
[57] K. Sun, P. Yang, Q. He, J. Tian, W. Duan, X. Wu, Y. Qu, H. Du, Weakly negative permittivity of MWCNT/TiN/CCTO ternary ceramics sintered in argon and nitrogen atmosphere, *Ceramics International*, 2021, **47**, 32297-32302, doi: 10.1016/j.ceramint.2021.08.124.
[58] Z. Zhang, M. Liu, M. M. Ibrahim, H. Wu, Y. Wu, Y. Li, G. A. M. Mersal, I. H. El Azab, S. M. El-Bahy, M. Huang, Y. Jiang, G. Liang, P. Xie, C. Liu, Flexible polystyrene/graphene composites with epsilon-near-zero properties, *Advanced Composites and Hybrid Materials*, 2022, **5**, 1054-1066, doi: 10.1007/s42114-022-00486-3.

